Band-edge exciton in quantum dots of semiconductors with a degenerate valence band: Dark and bright exciton states

Al. L. Efros and M. Rosen
Nanostructure Optics Section, Naval Research Laboratory, Washington D.C. 20375

M. Kuno, M. Nirmal, D. J. Norris, and M. Bawendi
Massachusetts Institute of Technology, 77 Massachusetts Avenue, Cambridge, Massachusetts 02139
(Received 12 March 1996)

We present a theoretical analysis of the band-edge exciton structure in nanometer-size crystallites of direct semiconductors with a cubic lattice structure or a hexagonal lattice structure which can be described within the framework of a quasicubic model. The lowest energy exciton, eightfold degenerate in spherically symmetric dots, is split into five levels by the crystal shape asymmetry, the intrinsic crystal field (in hexagonal lattice structures), and the electron-hole exchange interaction. Transition oscillator strengths and the size dependence of the splittings have been calculated. Two of the five states, including the ground state, are optically passive (dark excitons). The oscillator strengths of the other three levels (bright excitons) depend strongly on crystal size, shape, and energy band parameters. The relative ordering of the energy levels is also heavily influenced by these parameters. The distance between the first optically active state and the optically forbidden ground exciton state increases with decreasing size, leading to an increase of the Stokes shift in the luminescence. Our results are in good agreement with the size dependence of Stokes shifts obtained in fluorescence line narrowing and photoluminescence experiments in CdSe nanocrystals. Mixing of the dark and bright excitons in an external magnetic field allows the direct optical recombination of the dark exciton ground state. The observed shortening of the luminescence decay time in CdSe nanoncrystals in a magnetic field is also in excellent agreement with the theory, giving further support to the validity of our model. [S0163-1829(96)05831-6]

I. INTRODUCTION

Size dependent optical spectroscopy of semiconductor quantum dots has now reached the state held by magneto-optical spectroscopy during the mid-1960s, when the availability of high quality semiconductor materials on the one hand, and the development of the multiband Landau level theory by Pidgeon and Brown[1] on the other hand, enabled the description of the magnetic field dependence of the very complicated absorption spectra of zinc-blende semiconductors (see, for example, the review by Aggarwal[2]). The high quality of recently available nanosize CdSe crystals has allowed one to resolve and study the size dependence of up to eight excited states in their absorption spectra.[3–5] These excitation spectra, obtained in the strong confinement regime where the nanocrystals are small compared to the exciton Bohr radius, are the result of transitions between discrete quantum size levels of electrons and holes.[6,7] The small value of the crystal field splitting in CdSe (25 meV) allows one to consider this semiconductor as a zinc-blende material as a first approximation.[8] As a result, multiband effective mass theory which takes the degenerate valence band structure into account[9] has successfully described excitation spectra obtained in absorption,[3] hole burning, [4] and photoluminescence excitation experiments.[5,10,11]

The data on CdSe quantum dots, however, also provided us with a number of puzzles. While the large scale structure of the absorption spectra is now fairly well understood,[3–5,10,11] the nature of the emitting state has remained controversial. The photoluminescence of high quality samples with high quantum yield is found to be redshifted with respect to the excitation frequency and has an unusually long radiative lifetime[12] ($\tau_R \sim 1\,\mu$s at 10 K) compared to the bulk exciton recombination time ($\tau_R \sim 1$ ns). Simple parabolic band theory cannot explain these data in terms of recombination through internal states. Rather, band-edge emission in II-VI quantum dots (QD's) was explained as a surface effect and attributed to the recombination of weakly overlapping, surface-localized carriers.[12,13] These two effects can also be explained if the ground exciton were the optically forbidden state split from the first optically active state by the electron-hole exchange interaction.[14–18] Another puzzle is the very large Stokes shift of the luminescence with respect to the absorption for excitation far from the band edge, whose magnitude reaches $\sim$100 meV in 16 Å CdSe crystals,[12] while the Stokes shift of the resonant band-edge photoluminescence is only $\sim$9 meV.

In this paper we present a realistic multiband calculation of the band-edge exciton fine structure in quantum dots of semiconductors having a degenerate valence band, which takes into account the effect of the electron-hole exchange interaction, nonsphericity of the crystal shape, and the intrinsic hexagonal lattice asymmetry. We predict and describe a size dependent Stokes shift of both the resonant and nonresonant photoluminescence and the fine structure in absorption and hole burning spectra, and predict the formation of a long-lived dark exciton.[20] We show below that fluorescence line narrowing (FLN) and photoluminescence (PL) spectra in CdSe quantum dots support the picture of dark exciton formation via excitation of higher energy fine structure states followed by rapid thermalization to the exciton ground state. Particularly strong confirmation of our model is found in the

magnetic field dependence of the dark exciton decay time.[16]

In Sec. II we calculate the energy structure of the band-edge exciton and obtain transition oscillator strengths. We also calculate the lifetime of the optically passive ground exciton state in an external magnetic field. In Sec. III we present data on the size dependence of the resonant and nonresonant photoluminescence Stokes shift and on the magnetic field dependence of the dark exciton decay time in CdSe quantum dots. The experimental results are compared with theory in Sec. IV and conclusions are drawn from this comparison.

II. THEORY

In semiconductor crystals which are smaller than the bulk exciton Bohr radius, the energy spectrum and the wave functions of electron-hole pairs can be approximated using the independent quantization of the electron and hole motion (the so-called strong confinement regime). The electron and hole quantum confinement energies and their wave functions are found in the framework of the multiband effective mass approximation.[19] The formal procedure in deriving this method demands that the external potential be smooth enough. In the case of nanosize semiconductor crystals this leads to the condition $2a \gg a_0$, where a is the crystal radius and a_0 is the lattice constant. In addition, the effective mass approximation holds only if the typical energies of the electron and hole are close enough to the bottom of the conduction band and to the top of the valence band. In practice, this means that the quantization energy must be much smaller than the distance in energy to the next higher (lower) energy extremum in the conduction (valence) band.

In the framework of the effective mass approximation, for spherically symmetric crystals, i.e., finite size spherical crystals having a cubic lattice structure, the first quantum size level of electrons is a $1S_e$ state doubly degenerate with respect to its spin projection and the first quantum size level of holes is a $1S_{3/2}$ state which is fourfold degenerate with respect to the projection of its total angular momentum $\mathcal{K}$ ($M=3/2$, $1/2$, $-1/2$, and $-3/2$).[9,3] The energies and wave functions of these quantum size levels are easily found in the parabolic approximation. For electrons they are

$$E_{1S}=\frac{\hbar^2\pi^2}{2m_e a^2},$$

$$\psi_\alpha(\mathbf{r})=\xi(\mathbf{r})|S\alpha\rangle=\sqrt{\frac{2}{a}}\frac{\sin(\pi r/a)}{r}Y_{00}(\Omega)|S\alpha\rangle, \quad (1)$$

where m_e is the electron effective mass, a is the radius of the crystal, $Y_{lm}(\Omega)$ are spherical harmonic functions, $|S\alpha\rangle$ are the Bloch functions of the conduction band, and $\alpha=\uparrow(\downarrow)$ is the projection of the electron spin, $s_z=+(-)1/2$. For holes in the fourfold degenerate valence band they can be written

$$E_{3/2}(\beta)=\frac{\hbar^2\varphi^2(\beta)}{2m_{\rm hh}a^2}, \quad (2)$$

$$\psi_M(\mathbf{r})=2\sum_{l=0,2}R_l(r)(-1)^{M-3/2}\times\sum_{m+\mu=M}\begin{pmatrix}3/2 & l & 3/2\\ \mu & m & -M\end{pmatrix}Y_{lm}(\Omega)u_\mu, \quad (3)$$

where $\beta=m_{\rm lh}/m_{\rm hh}$ is the ratio of the light to heavy hole effective masses, $\varphi(\beta)$ is the first root of the equation[21–24,8]

$$j_0(\varphi)j_2(\sqrt{\beta}\varphi)+j_2(\varphi)j_0(\sqrt{\beta}\varphi)=0, \quad (4)$$

where $j_n(x)$ are spherical Bessel functions, $\begin{pmatrix}i & k & l\\ m & n & p\end{pmatrix}$ are Wigner $3j$ symbols, and u_μ ($\mu=\pm1/2,\pm3/2$) are the Bloch functions of the fourfold degenerate valence band Γ_8:[25]

$$u_{3/2}=\frac{1}{\sqrt{2}}(X+iY)\uparrow,\quad u_{-3/2}=\frac{i}{\sqrt{2}}(X-iY)\downarrow,$$

$$u_{1/2}=\frac{i}{\sqrt{6}}[(X+iY)\downarrow-2Z\uparrow], \quad (5)$$

$$u_{-1/2}=\frac{1}{\sqrt{6}}[(X-iY)\uparrow+2Z\downarrow].$$

The radial functions $R_l(r)$ are[21,23,8]

$$R_2(r)=\frac{A}{a^{3/2}}\left[j_2(\varphi r/a)+\frac{j_0(\varphi)}{j_0(\varphi\sqrt{\beta})}j_2(\varphi\sqrt{\beta}r/a)\right],$$

$$R_0(r)=\frac{A}{a^{3/2}}\left[j_0(\varphi r/a)-\frac{j_0(\varphi)}{j_0(\varphi\sqrt{\beta})}j_0(\varphi\sqrt{\beta}r/a)\right], \quad (6)$$

where the constant A is determined by the normalization condition

$$\int dr r^2[R_0^2(r)+R_2^2(r)]=1. \quad (7)$$

The dependence of φ on β is presented in Fig. 1(a).[8]

For spherical dots the exciton ground state ($1S_{3/2}1S_e$) is eightfold degenerate. However, shape and internal crystal structure anisotropy together with the electron-hole exchange interaction lift this degeneracy. The splitting and the transition oscillator strengths of the states, as well as their order, are very sensitive to crystal size and shape, as shown below. We calculate this splitting neglecting the warping of the valence band and the nonparabolicity of the electron and light hole energy spectra.

A. Energy spectrum and wave functions

Nanocrystal asymmetry lifts the hole state degeneracy. The asymmetry has two sources: the intrinsic asymmetry of the hexagonal lattice structure of the crystal[8] and the nonspherical shape of the finite crystal.[26] Both split the fourfold degenerate hole state into two twofold degenerate states—a Kramers doublet—having $|M|=1/2$ and $3/2$, respectively.

The splitting due to the intrinsic hexagonal lattice structure, $\Delta_{\rm int}$, can be written[8]

$$\Delta_{\rm int}=\Delta_{\rm cr}v(\beta), \quad (8)$$

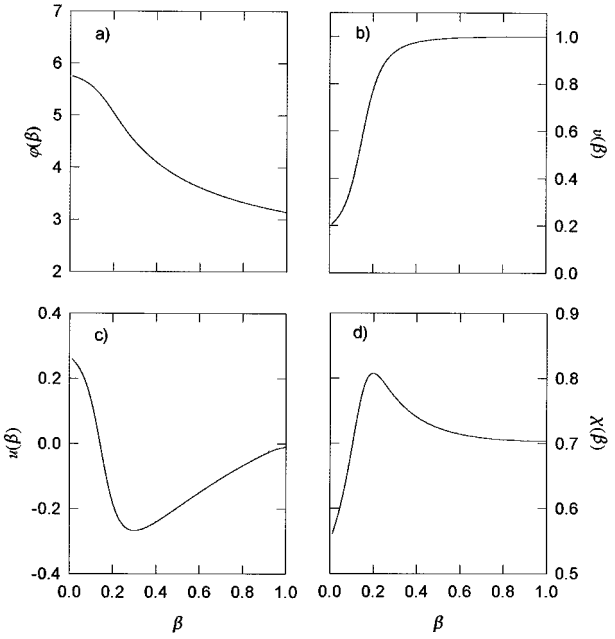

FIG. 1. (a) The dependence of the hole ground state function $\varphi(\beta)$ on the light to heavy hole effective mass ratio β; (b) the dimensionless function $v(\beta)$ associated with hole level splitting due to hexagonal lattice structure; (c) the dimensionless function $u(\beta)$ associated with hole level splitting due to crystal shape asymmetry; (d) the dimensionless function $\chi(\beta)$ associated with exciton splitting due to the electron-hole exchange interaction.

where Δ_{cr} is the crystal field splitting equal to the distance between the A and B valence subbands in bulk semiconductors having a hexagonal lattice structure (25 meV in CdSe). Equation (8) is obtained within the framework of the quasicubic model for the case when the crystal field splitting can be considered as a perturbation.[8] The Kramers doublet splitting does not depend on crystal size but only on the ratio of the light to heavy hole effective masses. The dimensionless function $v(\beta)$ describing this dependence,[8] shown in Fig. 1(b), varies rapidly in the region $0<\beta<0.3$. The $|M|=3/2$ state is the ground state.

We model the nonsphericity of the crystal by taking it to be an ellipsoid whose deviation from sphericity is characterized by the ratio $c/b=1+\mu$ of its major to minor axes. Here μ is the ellipticity of the crystal and is positive (negative) for prolate (oblate) crystals. The splitting arising from this deviation has been calculated in first order perturbation theory:[26]

$$\Delta_{sh}=2\mu u(\beta)E_{3/2}(\beta), \tag{9}$$

where $E_{3/2}$ is the $1S_{3/2}$ ground state hole energy for spherical crystals of radius $a=(b^2c)^{1/3}$. $E_{3/2}$ is inversly proportional to a^2 [see Eq. (2)] and the shape splitting is therefore a sensitive function of the crystal size. The function $u(\beta)$ (Ref. 26) decreases from a value of 4/15 at $\beta=0$, changes sign at $\beta=0.14$, and goes to zero at $\beta=1$ [see Fig. 1(c)].

The net splitting of the hole state, $\Delta(a,\beta,\mu)$, is the sum of the crystal field and shape splitting,

$$\Delta(a,\beta,\mu)=\Delta_{sh}+\Delta_{int}. \tag{10}$$

In crystals where the function $u(\beta)$ is negative, e.g., in CdSe crystals where $\beta=0.28$,[5] the net splitting decreases with size in prolate ($\mu>0$) crystals. Even the order of the hole levels can change, with the $|M|=1/2$ state becoming the hole ground level for sufficiently small crystals.[27] This can be qualitatively understood within a model of uncoupled A and B valence subbands. In prolate crystals the energy of the lowest hole quantum size level is determined by its motion in the plane perpendicular to the hexagonal axis. In this plane the hole effective mass in the lowest subband A is smaller than that in the higher B subband.[8] Decreasing the size of the crystal causes a shift of the quantum size level inversely proportional to both the effective mass and the square of the nanocrystal radius. The shift is therefore larger for the A subband than for the B subband and, as a result, can change the order of the levels in small crystals. In oblate ($\mu<0$) crystals, where the levels are determined by motion along the hexagonal axis, the B subband has the smaller mass. Hence the net splitting increases with decreasing size and the states maintain their original order.

The eightfold degeneracy of the spherical band-edge exciton is also broken by the electron-hole exchange interaction which mixes different electron and hole spin states. It has the following form:[28,25]

$$\hat{H}_{exch}=-(2/3)\varepsilon_{exch}(a_0)^3\delta(\mathbf{r}_e-\mathbf{r}_h)\boldsymbol{\sigma}J, \tag{11}$$

where σ is the electron Pauli spin-1/2 matrix, J is the hole spin-3/2 matrix, a_0 is the lattice constant, and ε_{exch} is the exchange strength constant. In bulk crystals with cubic lattice structure this term splits the eightfold degenerate ground exciton state into a fivefold degenerate optically passive state with total angular momentum 2 and a threefold degenerate optically active state with total angular momentum 1. This splitting can be expressed in terms of the bulk exciton Bohr radius a_{ex}:

$$\hbar\omega_{ST}=(8/3\pi)(a_0/a_{ex})^3\varepsilon_{exch}. \tag{12}$$

In bulk crystals with hexagonal lattice structure this term splits the exciton fourfold degenerate ground state into a triplet and a singlet state, separated by

$$\hbar\omega_{ST}=(2/\pi)(a_0/a_{ex})^3\varepsilon_{exch}. \tag{13}$$

Equations (12) and (13) allow one to evaluate the exchange strength constant. In CdSe crystals, where $\hbar\omega_{ST}=0.13$ meV,[29] a value of $\varepsilon_{exch}=450$ meV is obtained using $a_{ex}=56$ Å.

Taken together, the hexagonal lattice structure, crystal shape asymmetry, and electron-hole exchange interaction split the original ''spherical'' eightfold degenerate exciton into five levels. The levels are labeled by the magnitude of the exciton total angular momentum projection, $F=M+s_z$: one level with $F=\pm2$, two with $F=\pm1$, and two with $F=0$. The level energies $\varepsilon_{|F|}$ are determined by solving the secular equation $\det(\hat{E}-\varepsilon_{|F|})=0$, where the matrix $\hat{E}$ consists of matrix elements of the asymmetry perturbations and the exchange interaction $\hat{H}_{exch}$, taken between the exciton wave functions $\Psi_{\alpha,M}(\mathbf{r}_e,\mathbf{r}_h)=\psi_\alpha(\mathbf{r}_e)\psi_M(\mathbf{r}_h)$:

	↑,3/2	↑,1/2	↑,−1/2	↑,−3/2	↓,3/2	↓,1/2	↓,−1/2	↓,−3/2
↑,3/2	$\frac{-3\eta}{2}-\frac{\Delta}{2}$	0	0	0	0	0	0	0
↑,1/2	0	$\frac{-\eta}{2}+\frac{\Delta}{2}$	0	0	$-i\sqrt{3}\eta$	0	0	0
↑,−1/2	0	0	$\frac{\eta}{2}+\frac{\Delta}{2}$	0	0	$-i2\eta$	0	0
↑,−3/2	0	0	0	$\frac{3\eta}{2}-\frac{\Delta}{2}$	0	0	$-i\sqrt{3}\eta$	0
↓,3/2	0	$i\sqrt{3}\eta$	0	0	$\frac{3\eta}{2}-\frac{\Delta}{2}$	0	0	0
↓,1/2	0	0	$i2\eta$	0	0	$\frac{\eta}{2}+\frac{\Delta}{2}$	0	0
↓,−1/2	0	0	0	$i\sqrt{3}\eta$	0	0	$\frac{-\eta}{2}+\frac{\Delta}{2}$	0
↓,−3/2	0	0	0	0	0	0	0	$\frac{-3\eta}{2}-\frac{\Delta}{2}$

(14)

$\eta=(a_{ex}/a)^3\hbar\omega_{ST}\chi(\beta)$, and the dimensionless function $\chi(\beta)$ is written in terms of the electron and hole radial wave functions,

$$\chi(\beta)=(1/6)a^2\int_0^a dr\ \sin^2(\pi r/a)[R_0^2(r)+0.2R_2^2(r)]. \tag{15}$$

The dependence of χ on the parameter β is shown in Fig. 1(d).

Solution of the secular equation yields five exciton levels. The energy of the exciton with total angular momentum projection $|F|=2$ and its dependence on crystal size are given by

$$\varepsilon_2=-3\eta/2-\Delta/2. \tag{16}$$

The respective wave functions are

$$\Psi_{-2}(\mathbf{r}_e,\mathbf{r}_h)=\Psi_{\downarrow,-3/2}(\mathbf{r}_e,\mathbf{r}_h),$$

$$\Psi_2(\mathbf{r}_e,\mathbf{r}_h)=\Psi_{\uparrow,3/2}(\mathbf{r}_e,\mathbf{r}_h). \tag{17}$$

The energies and size dependence of the two levels, each with total momentum projection $|F|=1$, are given by

$$\varepsilon_1^{U,L}=\eta/2\pm\sqrt{(2\eta-\Delta)^2/4+3\eta^2}, \tag{18}$$

where U and L correspond to the upper (''+'' in this equation) or lower (''−'' in this equation) sign, respectively. We denote these states by $\pm1^U$ and $\pm1^L$, respectively; i.e., the upper and lower state with projection $F=\pm1$. The corresponding wave functions for the states with $F=+1$ are

$$\Psi_1^{U,L}(\mathbf{r}_e,\mathbf{r}_h)=\mp iC^+\Psi_{\uparrow,1/2}(\mathbf{r}_e,\mathbf{r}_h)+C^-\Psi_{\downarrow,3/2}(\mathbf{r}_e,\mathbf{r}_h); \tag{19}$$

for the states with $F=-1$

$$\Psi_{-1}^{U,L}(\mathbf{r}_e,\mathbf{r}_h)=\mp iC^-\Psi_{\uparrow,-3/2}(\mathbf{r}_e,\mathbf{r}_h)+C^+\Psi_{\downarrow,-1/2}(\mathbf{r}_e,\mathbf{r}_h), \tag{20}$$

where

$$C^{\pm}=\sqrt{\frac{\sqrt{f^2+d}\pm f}{2\sqrt{f^2+d}}}, \tag{21}$$

$f=(-2\eta+\Delta)/2$, and $d=3\eta^2$. The energies and size dependence of the two $F=0$ exciton levels are given by

$$\varepsilon_0^{U,L}=\eta/2+\Delta/2\pm2\eta \tag{22}$$

(we denote the two $F=0$ states by 0^U and 0^L), with corresponding wave functions

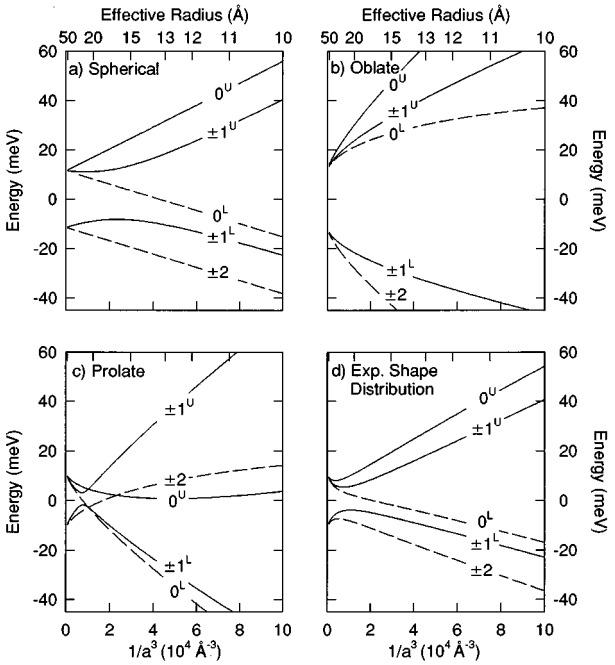

FIG. 2. The size dependence of the exciton band-edge structure in ellipsoidal hexagonal CdSe quantum dots with ellipticity μ: (a) spherical dots ($\mu=0$); (b) oblate dots ($\mu=-0.28$); (c) prolate dots ($\mu=0.28$); (d) dots having a size dependent ellipticity as determined from SAXS and TEM measurements. Solid (dashed) lines indicate optically active (passive) levels.

$$\Psi_0^{U,L}(\mathbf{r}_e,\mathbf{r}_h)=\frac{1}{\sqrt{2}}[\mp i\Psi_{\uparrow,-1/2}(\mathbf{r}_e,\mathbf{r}_h)+\Psi_{\downarrow,1/2}(\mathbf{r}_e,\mathbf{r}_h)], \tag{23}$$

The size dependence of the band-edge exciton splitting for hexagonal CdSe crystals with different shapes is shown in Fig. 2. The calculation was done using $\beta=0.28$.[5] In spherical crystals [Fig. 2(a)] the $F=\pm 2$ state is the exciton ground state for all sizes, and is optically passive, as was shown in Ref. 8. The separation between the ground state and the lower optically active $F=\pm 1$ state initially increases with decreasing size as $1/a^3$, but tends to $3\Delta/4$ for very small crystals. In oblate crystals [Fig. 2(b)] the order of the exciton levels is the same as in spherical ones. However, the splitting does not saturate, because in these crystals Δ increases with decreasing size. In prolate crystals Δ becomes negative with decreasing size and this changes the order of the exciton levels at some value of the radius [Fig. 2(c)]; in small crystals the optically passive (as we show below) $F=0$ state becomes the ground exciton state. The crossing occurs when Δ goes through 0. In nanocrystals of this size the shape asymmetry exactly compensates the asymmetry connected with the hexagonal lattice structure,[27] and hence the exciton levels have ''spherical'' symmetry. As a result there is one fivefold degenerate exciton with total angular momentum 2 (which is reflected in the crossing of the 0^L, $\pm 1^L$, and ± 2 levels) and one threefold degenerate exciton state with total angular momentum 1 (reflected in the crossing of the 0^U and $\pm 1^U$ levels). In Fig. 2(d) the band-edge exciton fine structure is shown for the case where the ellipticity varies with size,[30] corresponding to small-angle x-ray scattering (SAXS) and transmission electron microscopy (TEM) measurements of our CdSe crystals.[31] The level structure closely resembles that of spherical crystals.

The size dependence of the band-edge exciton splitting in cubic CdTe crystals with different shapes is shown in Fig. 3. The calculation was done using the parameters $\beta=0.086$ and $\hbar\omega_{\mathrm{ST}}=0.04$ meV. One can see that in the spherical nanocrystals the electron-hole exchange interaction splits the eightfold degenrate band-edge exciton into a fivefold degenerate exciton with total angular momentum 2 and a threefold degenerate exciton with total angular momentum 1 [Fig. 3(a)]. Crystal shape asymmetry lifts the degeneracy of these states and completely determines the relative order of the exciton states [see Fig. 3(b) and Fig. 3(c) for comparison].

B. Selection rules and transition oscillator strengths

To describe the fine structure of the absorption spectra and photoluminescence we calculate transition oscillator strengths for these five exciton states. The mixing of the electron and hole spin momentum states by the electron-hole exchange interaction strongly affects the optical transition probabilities. The wave functions of the $|F|=2$ exciton state, however, are unaffected by this interaction [see Eq. (17)]; it is optically passive in the dipole approximation because emitted or absorbed photons cannot have an angular momentum projection of ± 2. The probability of optical excitation or recombination of an exciton state with total angular momentum projection F is proportional to the square of the matrix element of the momentum operator $\mathbf{e}\hat{\mathbf{p}}$ between that state and the vacuum state,

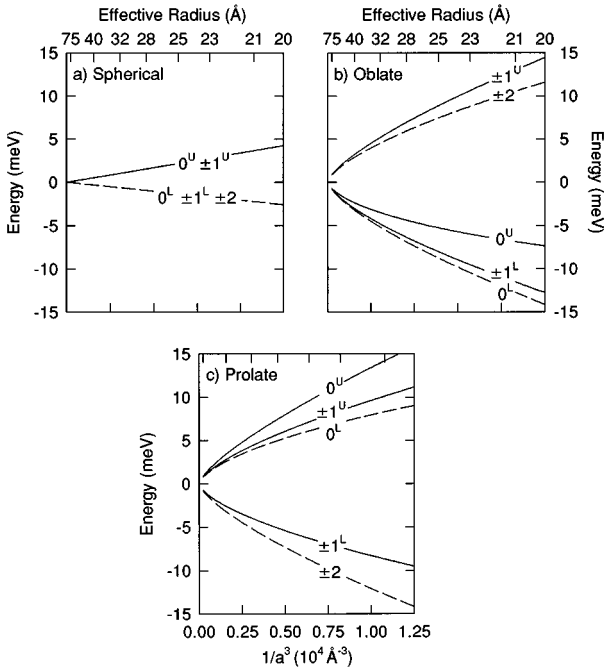

FIG. 3. The size dependence of the exciton band-edge structure in ellipsoidal cubic CdTe quantum dots with ellipticity μ: (a) spherical dots ($\mu=0$); (b) oblate dots ($\mu=-0.28$); (c) prolate dots ($\mu=0.28$); Solid (dashed) lines indicate optically active (passive) levels.

$$P_F=|\langle 0|\mathbf{e}\hat{\mathbf{p}}|\tilde{\Psi}_F\rangle|^2, \tag{24}$$

where $|0\rangle=\delta(\mathbf{r}_e-\mathbf{r}_h)$, $\mathbf{e}$ is the polarization vector of the emitted or absorbed light, the momentum operator $\hat{\mathbf{p}}$ acts only on the valence band Bloch functions [see Eq. (5)] and the exciton wave function $\tilde{\Psi}_F$ is written in the electron-electron representation. Exciton wave functions in the electron-hole representation are transformed to the electron-electron representation by taking the complex conjugate of Eqs. (17), (19), and (23) and flipping the spin projections in the hole Bloch functions ($\uparrow$ and $\downarrow$ to $\downarrow$ and $\uparrow$).

For the exciton state with $F=0$ we obtain

$$P_0^{U,L}=|\langle 0|\mathbf{e}\hat{\mathbf{p}}|\tilde{\Psi}_0^{U,L}\rangle|^2=\frac{(1\pm 1)^2}{3}KP^2\cos^2(\theta), \tag{25}$$

where $P=\langle S|\hat{p}_z|Z\rangle$ is the Kane interband matix element, θ is the angle between the polarization vector of the emitted or absorbed light and the hexagonal axis of the crystal, and K is the square of the overlap integral[8]

$$K=\frac{2}{a}\left|\int dr\, r\,\sin(\pi r/a)R_0(r)\right|^2. \tag{26}$$

Its value is independent of crystal size and depends only on β; hence the excitation probability of the $F=0$ state does not depend on crystal size. For the lower exciton state, 0^L, it is identically zero. At the same time the exchange interaction increases the excitation probability of the upper 0^U exciton

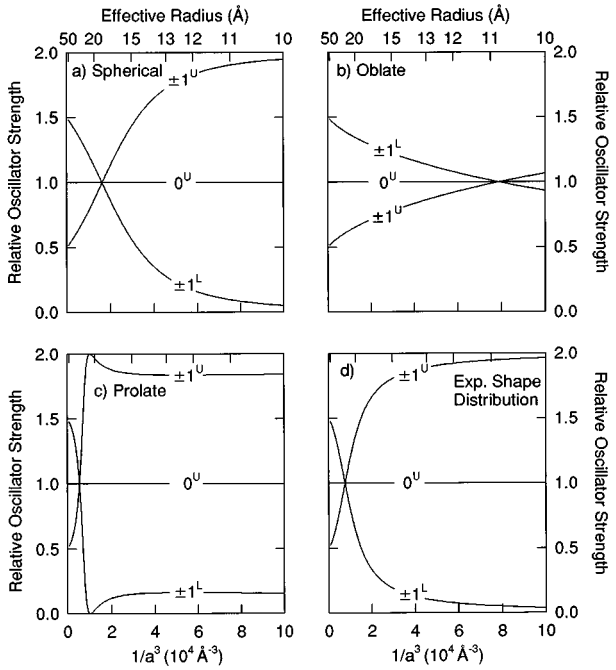

FIG. 4. The size dependence of the oscillator strengths, relative to that of the 0^U state, for the optically active states in hexagonal CdSe quantum dots with ellipticity μ: (a) spherical dots ($\mu=0$); (b) oblate dots ($\mu=-0.28$); (c) prolate dots ($\mu=0.28$); (d) dots having a size dependent ellipticity as determined from SAXS and TEM measurements.

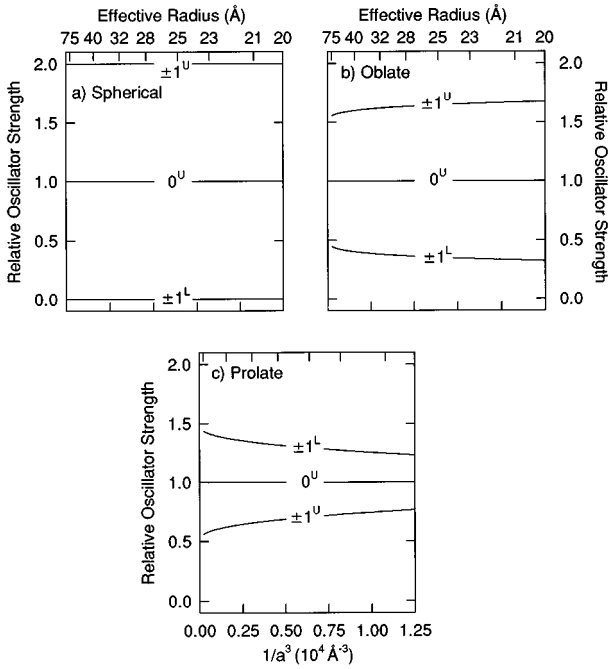

FIG. 5. The size dependence of the oscillator strengths, relative to that of the 0^U state, for the optically active states in cubic CdTe quantum dots with ellipticity μ: (a) spherical dots ($\mu=0$); (b) oblate dots ($\mu=-0.28$); (c) prolate dots ($\mu=0.28$).

state by a factor of 2. This result arises from the constructive and destructive interference of the wave functions of the two indistinguishable exciton states $|\uparrow,-1/2\rangle$ and $|\downarrow,1/2\rangle$ [see Eq. (23)].

For the exciton state with $F=1$ we obtain

$$P_1^{U,L}=\frac{1}{3}\left(\frac{2\sqrt{f^2+d}\mp f\pm\sqrt{3d}}{2\sqrt{f^2+d}}\right)KP^2\sin^2(\theta). \qquad (27)$$

The excitation probability of the $F=-1$ state is equal to that of the $F=1$ state. As a result, the total transition probability to the doubly degenerate $|F|=1$ exciton states is equal to $2P_1^{U,L}$.

Equations (25) and (27) show that the $F=0$ and $|F|=1$ state excitation probabilities differ in their dependence on the angle between the light polarization vector and the hexagonal axis of the crystal. If the crystal hexagonal axes are aligned perpendicular to the light direction, only the active $F=0$ state can be excited. Alternatively, when the crystals are aligned along the light propagation direction, only the upper and lower $|F|=1$ states will participate in the absorption. For the case of randomly oriented crystals, polarized excitation resonant with one of these exciton states selectively excites suitably oriented crystals, leading to polarized luminescence.[8] Observation of this effect has been reported in several papers.[12,32,15] Furthermore, a large energy splitting between the $F=0$ and $|F|=1$ states can lead to different Stokes shifts in the polarized luminescence.

To find the probability of exciton excitation for a system of randomly oriented nanocrystals, we average Eqs. (25) and (27) over all possible solid angles. The respective excitation probabilities are proportional to

$$\overline{P_0^{U,L}}=\frac{(1\pm1)^2KP^2}{9},$$

$$\overline{P_1^{U,L}}=\overline{P_{-1}^{U,L}}=\frac{2KP^2}{9}\left(\frac{2\sqrt{f^2+d}\mp f\pm\sqrt{3d}}{2\sqrt{f^2+d}}\right). \qquad (28)$$

There are three optically active states with relative oscillator strengths $\overline{P_0^U}$, $2\overline{P_1^U}$, and $2\overline{P_1^L}$. The dependence of these strengths on size for different shapes is shown in Fig. 4 for hexagonal CdSe crystals. It is seen that the crystal shape strongly influences this dependence. For example, in prolate crystals [Fig. 4(c)] the $\pm1^L$ state oscillator strength goes to zero for those crystals for which $\Delta=0$; i.e., where the crystal shape asymmetry exactly compensates the internal asymmetry connected with the hexagonal lattice structure. For these crystals the oscillator strengths of all the upper states (0^U, 1^U, and -1^U) are equal. Nevertheless, one can see that for all nanocrystal shapes the excitation probability of the lower $|F|=1$ ($\pm1^L$) exciton state, $2\overline{P_1^L}$, decreases with size and that the upper $|F|=1$ ($\pm1^U$) gains its oscillator strength.

This can be understood by examining the spherically symmetric limit. In spherical nanocrystals the exchange interaction leads to the formation of two exciton states—with total angular momenta 2 and 1. The ground state is the optically passive state with total angular momentum 2. This state is fivefold degenerate with respect to the total angular momentum projection. For small nanocrystals the splitting of the exciton levels due to the nanocrystal asymmetry can be considered as a perturbation to the exchange interaction, which

grows as $1/a^3$. In this situation the wave functions of the $\pm 1^L$, 0^L, and ± 2 exciton states turn into the wave functions of the optically passive exciton with total angular momentum 2. The wave functions of the $\pm 1^U$ and 0^U exciton states become those of the optically active exciton states with total angular momentum 1. These three states therefore carry nearly all the oscillator strength.

In large crystals, for all possible shapes, we can neglect the exchange interaction (which decreases as $1/a^3$), and thus there are only two fourfold degenerate exciton states (see Fig. 3). The splitting here is determined by the shape asymmetry and the intrinsic crystal field. In a system of randomly oriented crystals, the excitation probability of both these states is the same: $\overline{P_0^U}+2\overline{P_1^U}=2\overline{P_1^L}=2KP^2/3$.[8]

In Fig. 5 we show these dependences for variously shaped cubic CdTe nanocrystals.

It is necessary to note here that despite the fact that the exchange interaction drastically changes the structure and the oscillator strengths of the band-edge exciton, the polarization properties of the nanocrystal are determined by the internal and crystal shape asymmetries. All polarization effects are proportional to the net splitting parameter Δ and go to zero when $\Delta=0$.

C. Recombination of the dark exciton in magnetic fields

Time decay measurements of the dark exciton in CdSe nanocrystals in the presence of external magnetic fields strongly support our model.[16] Recombination of the dark exciton is allowed if the magnetic field is not directed along the hexagonal axis of the nanocrystal. In this case F is no longer a good quantum number and the ± 2 dark exciton states are admixed with the optically active ± 1 bright exciton states. This now allows the direct optical recombination of the ± 2 exciton ground state.

For nanosize quantum dots the effect of an external magnetic field **H** is well described as a molecular Zeeman effect:

$$\hat{H}_H=\frac{1}{2}g_e\mu_B\boldsymbol{\sigma}\mathbf{H}-g_h\mu_B\mathscr{K}\mathbf{H}, \tag{29}$$

where g_e and g_h are the electron and hole g factors, respectively, and μ_B is the Bohr magneton. For electrons in CdSe $g_e=0.68$.[33] The value of the hole g factor is calculated in the Appendix using the results of Ref. 34, and is $g_h=-1.09$. In Eq. (29) we neglect the diamagnetic H^2 terms because the dots are significantly smaller than the magnetic length ($\sim$115 Å at 10 T).

Treating the magnetic interaction as a perturbation, we can determine the influence of the magnetic field on the unperturbed exciton state using the perturbation matrix $\hat{E}'_H=\langle\Psi_{\alpha,M}|\mu_B^{-1}\hat{H}_H|\Psi_{\alpha',M'}\rangle$:

	$\uparrow,3/2$	$\uparrow,1/2$	$\uparrow,-1/2$	$\uparrow,-3/2$	$\downarrow,3/2$	$\downarrow,1/2$	$\downarrow,-1/2$	$\downarrow,-3/2$
$\uparrow,3/2$	$\frac{H_z(g_e-3g_h)}{2}$	$\frac{-i\sqrt{3}g_hH_-}{2}$	0	0	$\frac{g_eH_-}{2}$	0	0	0
$\uparrow,1/2$	$\frac{i\sqrt{3}g_hH_+}{2}$	$\frac{H_z(g_e-g_h)}{2}$	$-ig_hH_-$	0	0	$\frac{g_eH_-}{2}$	0	0
$\uparrow,-1/2$	0	ig_hH_+	$\frac{H_z(g_e+g_h)}{2}$	$\frac{-i\sqrt{3}g_hH_-}{2}$	0	0	$\frac{g_eH_-}{2}$	0
$\uparrow,-3/2$	0	0	$\frac{i\sqrt{3}g_hH_+}{2}$	$\frac{H_z(g_e+3g_h)}{2}$	0	0	0	$\frac{g_eH_-}{2}$
$\downarrow,3/2$	$\frac{g_eH_+}{2}$	0	0	0	$\frac{-H_z(g_e+3g_h)}{2}$	$\frac{-i\sqrt{3}g_hH_-}{2}$	0	0
$\downarrow,1/2$	0	$\frac{g_eH_+}{2}$	0	0	$\frac{i\sqrt{3}g_hH_+}{2}$	$\frac{-H_z(g_e+g_h)}{2}$	$-ig_hH_-$	0
$\downarrow,-1/2$	0	0	$\frac{g_eH_+}{2}$	0	0	ig_hH_+	$\frac{-H_z(g_e-g_h)}{2}$	$\frac{-i\sqrt{3}g_hH_-}{2}$
$\downarrow,-3/2$	0	0	0	$\frac{g_eH_+}{2}$	0	0	$\frac{i\sqrt{3}g_hH_+}{2}$	$\frac{-H_z(g_e-3g_h)}{2}$

(30)

where H_z is the magnetic field projection along the crystal hexagonal axis and $H_\pm=H_x\pm iH_y$. One can see from Eq. (30) that components of the magnetic field perpendicular to the hexagonal crystal axis mix the $F=\pm 2$ dark exciton states with the respective optically active $F=\pm 1$ bright exciton states. In small nanocrystals, where η is of the order of 10 meV, the influence of even the strongest magnetic field can be considered as a perturbation. The case of large crystals where η is of the same order as $\mu_B g_e H$ will be considered later. The admixture in the $F=2$ state is given by

$$\Delta\Psi_2=\frac{\mu_B H_-}{2}\left[\frac{g_e C^- -\sqrt{3}g_h C^+}{\varepsilon_2-\varepsilon_1^+}\Psi_1^+ + \frac{\sqrt{3}g_h C^- + g_e C^+}{\varepsilon_2-\varepsilon_1^-}\Psi_1^-\right], \tag{31}$$

where the constants $C^{\pm}$ are given in Eq. (21). The admixture in the $F=-2$ exciton state of the $F=-1$ exciton state is described similarly.

This admixture of the optically active bright exciton states allows the optical recombination of the dark exciton. The radiative recombination rate of an exciton state, F, can be obtained by summing Eq. (24) over all light polarizations:[35]

$$\frac{1}{\tau_{|F|}}=\frac{4e^2\omega n_r}{3m_0^2c^3\hbar}|\langle 0|\hat{p}_\mu|\tilde{\Psi}_F\rangle|^2, \tag{32}$$

where ω and c are the light frequency and velocity, n_r is the refractive index, and m_0 is the free electron mass. Using Eqs. (25)–(27) we obtain the radiative decay time for the upper exciton state with $F=0$,

$$\frac{1}{\tau_0}=\frac{8\omega n_r P^2 K}{9\times 137 m_0^2 c^2}; \tag{33}$$

for the upper and lower exciton states with $|F|=1$,

$$\frac{1}{\tau_1^{U,L}}=\left(\frac{2\sqrt{f^2+d}\mp f\pm\sqrt{3d}}{2\sqrt{f^2+d}}\right)\frac{1}{\tau_0}. \tag{34}$$

Using the admixture of the $|F|=1$ states in the $|F|=2$ exciton given in Eq. (31), we calculate the recombination rate of the $|F|=2$ exciton in a magnetic field,

$$\frac{1}{\tau_2(H)}=\frac{3\mu_B^2H^2\sin^2(\theta)}{8\Delta^2}\left(2g_h-g_e\frac{2\eta+\Delta}{3\eta}\right)^2\frac{1}{\tau_0}. \tag{35}$$

The characteristic time τ_0 does not depend on the crystal radius. For CdSe, calculations using $2P^2/m_0=17.5$ eV (Ref. 3) give $\tau_0=1.6$ ns.

In large crystals the magnetic field splitting $\mu_B g_e H$ is of the same order as the exchange interaction η and cannot be considered a perturbation. At the same time, both these energies are much smaller than the splitting due to the crystal asymmetry. We consider here the admixture in the $|F|=2$ dark exciton of the lowest $|F|=1$ exciton only. This can be calculated exactly. The magnetic field also lifts the degeneracy of the exciton states with respect to the sign of the total angular momentum projection F. The energies of the former $F=-2$ and $F=-1$ states are

$$\varepsilon_{-1,-2}^{\pm}=\frac{-\Delta+3\mu_B g_h H_z}{2} \pm\frac{\sqrt{(3\eta+\mu_B g_e H_z)^2+(\mu_B g_e)^2H_\perp^2}}{2}, \tag{36}$$

where + (−) refers to the $F=-1$ state with an $F=-2$ admixture ($F=-2$ state with an $F=-1$ admixture) and $H_\perp=\sqrt{H_x^2+H_y^2}$. The corresponding wave functions are

$$\Psi_{-1,-2}^{\pm}=\sqrt{\frac{\sqrt{p^2+|n|^2}\pm p}{2\sqrt{p^2+|n|^2}}}\Psi_{\uparrow,-3/2} \mp\frac{n}{\sqrt{2\sqrt{p^2+|n|^2}(\sqrt{p^2+|n|^2}\pm p)}}\Psi_{\downarrow,-3/2}, \tag{37}$$

where $n=\mu_B g_e H_+$ and $p=3\eta+\mu_B g_e H_z$. The energies and wave functions of the former $F=2,1$ states are (using notation similar to that used just above)

$$\varepsilon_{1,2}^{\pm}=\frac{-\Delta-3\mu_B g_h H_z}{2}\pm\frac{\sqrt{(3\eta-\mu_B g_e H_z)^2+(\mu_B g_e)^2H_\perp^2}}{2}, \tag{38}$$

$$\Psi_{1,2}^{\pm}=\sqrt{\frac{\sqrt{p'^2+|n'|^2}\pm p'}{2\sqrt{p'^2+|n'|^2}}}\Psi_{\downarrow,3/2} \mp\frac{n'}{\sqrt{2\sqrt{p'^2+|n'|^2}(\sqrt{p'^2+|n'|^2}\pm p')}}\Psi_{\uparrow,3/2}, \tag{39}$$

where $n'=\mu_B g_e H_-$ and $p'=3\eta-\mu_B g_e H_z$. As a result the decay time of the dark exciton in an external magnetic field can be written

$$\frac{1}{\tau(H)}=\frac{\sqrt{1+\zeta^2+2\zeta\cos\theta}-1-\zeta\cos\theta}{2\sqrt{1+\zeta^2+2\zeta\cos\theta}}\frac{3}{2\tau_0}, \tag{40}$$

where $\zeta=\mu_B g_e H/3\eta$. The probabilty of exciton recombination increases in weak magnetic fields ($\zeta\ll 1$) as $[(0.5\mu_B g_e H)^2/(3\eta)^2][3\sin^2(\theta)/2\tau_0]$, and saturates in strong magnetic fields ($\zeta\gg 1$), reaching $[3(1-\cos\theta)/4\tau_0][1-(3\eta/\mu_B g_e H)(1+\cos\theta)]$.

One can see from Eqs. (35) and (40) that the recombination lifetime depends on the angle between the crystal hexagonal axis and the magnetic field. The recombination time is different for different crystal orientations, which leads to a nonexponetial time decay dependence for a system of randomly oriented crystals.

III. EXPERIMENT

The samples in our Stokes shift study were prepared using the synthetic technique described in Ref. 31. This method produces nearly monodisperse wurtzite crystallites of CdSe ($\sigma<5\%$) which are slightly prolate and have surfaces passivated by an organic layer of tri-*n*-octylphosphine/tri-*n*-octylphosphine oxide ligands. In total, 18 samples were prepared for this study. Their effective radii, as determined by small angle x-ray scattering and TEM measurements, range from 12 to 56 Å. The samples were isolated as a powder and redispersed into a mixture of *o*-terphenyl in tri-*n*-butylphosphine (200 mg/ml) to form an optically clear glass at liquid helium temperatures. Each sample was loaded between sapphire flats separated by a 0.5 mm thick Teflon

spacer and mounted in a helium cold finger cryostat for low temperature optical work. The 12 Å sample used in the magnetic field and luminescence decay experiments was left in its original growth solution without being redispersed in tri-*n*-butylphosphine and *o*-terphenyl. With the exception of the 12 Å sample just described, all the samples in our Stokes shift study were freshly prepared specifically for this study.

Absorption, luminescence, and fluorescence line narrowed spectra were taken on the same optical setup. In the absorption experiment, light from a 300 W Xe arc lamp was passed through the sample and the transmitted light detected with an optical multichannel analyzer (OMA) coupled to a 0.33 m single spectrometer. The full luminescence spectrum of each sample was obtained by passing light from a 300 W Hg-Xe arc lamp through a 0.25 m spectrometer and exciting it above its band edge. Typically, the excitation light was kept spectrally broad [50 nm full width at half maximum (FWHM)] to prevent any possible size selection of the dots. The emitted light was then dispersed and detected with the spectrometer/OMA combination described in the absorption experiment.

Fluorescence line narrowed spectra were acquired by exciting the samples with the output of a *Q*-switched neodymium-doped yttrium aluminum garnet (Nd:YAG)/dye laser system ($\sim$7 ns pulses). The laser power was attenuated to ensure that the luminescence varied linearly with the excitation intensity. The measured luminescence was dispersed and detected with a 0.33 m spectrometer coupled to a 5 ns gated OMA.

Magnetic field studies were conducted by placing the sample within the bore of a variable field superconducting magnet. The excitation source was the Nd:YAG/dye laser system described above. The resulting luminescence was dispersed through a 0.66 m single spectrometer and detected with a 5 ns time gated OMA. Luminescence decays were recorded with the following: a 500 Mhz digitizing oscilloscope, a photomultiplier tube with 2 ns resolution, and a 0.75 m subtractive double spectrometer to eliminate scattered laser light.

A. Stokes shift of the resonant photoluminescence

We observe strong evidence for the predicted band-edge fine structure in our fluorescence line narrowing (FLN) experiments. By exciting our samples on the red edge of the absorption, we selectively excite the largest dots present in the residual size distribution of each sample. This reduces the inhomogeneous broadening of the luminescence and the resulting emission is spectrally narrow, displaying a well resolved longitudinal optical (LO) phonon progression. In practice, we excite our samples at that point on their red edge where the absorption is roughly 1/3 of the peak of the band-edge absorption. Figure 6 shows the FLN spectra for the size series considered in this paper. The peak of the zero LO phonon line (ZPL) is observed to be shifted with respect to the excitation energy. This Stokes shift is size dependent and ranges from $\sim$20 meV for small crystals to $\sim$2 meV for large crystals. Moving the excitation position does not noticeably affect the Stokes shift of the larger samples; however, it does make a difference for the smaller sizes. We attribute this difference to the excitation of different size dots within the size distribution of a sample, causing the observed Stokes shift to change. The effect is largest in the case of small nanocrystallites because of the size dependence of the Stokes shift (see Fig. 7).

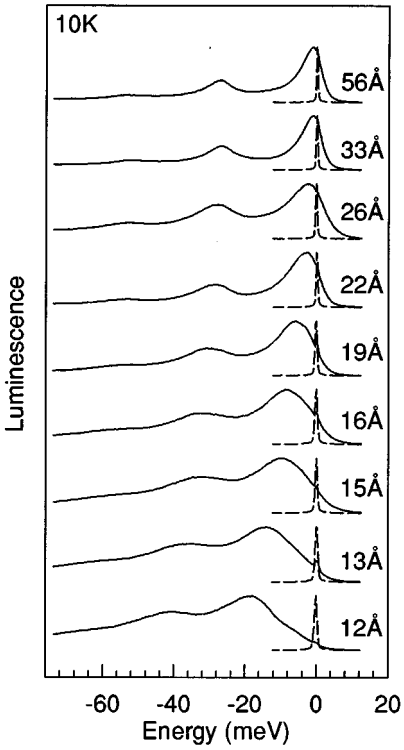

FIG. 6. Normalized FLN spectra for CdSe QD's between 12 and 56 Å in radius. The mean radii of the dots are determined from SAXS and TEM measurements. A 10 Hz *Q*-switched Nd:YAG/dye laser system ($\sim$7 ns pulses) serves as the excitation source. Detection of the FLN signal is accomplished using a time gated OMA. The laser line is included in the figure (dotted line) for reference purposes. All FLN spectra are taken at 10 K.

In terms of the proposed model, excitation on the red edge of the absorption probes the lowest $|F|=1$ bright exciton state [see Fig. 2(d)]. The transition to this state is followed by thermal relaxation to the dark $|F|=2$ state, from where recombination occurs through a phonon assisted[16,8] or nuclear/paramagnetic spin-flip assisted transition.[16] The observed Stokes shift is the difference in energy between the $\pm 1^L$ state and the dark ± 2 state and increases with decreasing size.

We find good agreement between the experimental values of the size dependent Stokes shift and the values derived from theory. Figure 7 compares the two results. The only parameters used in the theoretical calculation are taken from the literature: $a_{\mathrm{ex}}=56$ Å,[3] $\hbar\omega_{\mathrm{ST}}=0.13$ meV,[29] and $\beta=0.28$.[4,5] The comparison shows that there is good quantitative agreement between experiment and theory for large sizes. For small crystals, however, the theoretical splitting based on the size dependent exchange interaction begins to underestimate the observed Stokes shift. This discrepancy may be explained, in part, by an additional contribution to the Stokes shift by phonons, which is not accounted for in the present model.[36,37]

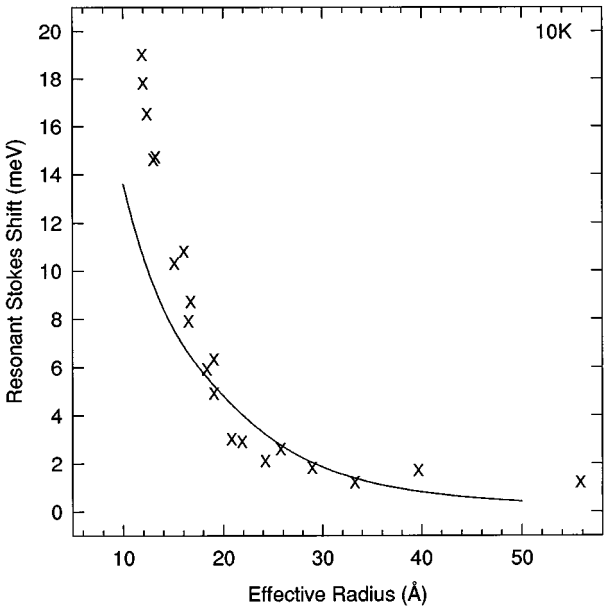

FIG. 7. The size dependence of the resonant Stokes shift. This Stokes shift is the difference in energy between the pump energy and the peak of the ZPL in the FLN measurement. The points labeled $\times$ are the experimental values. The solid line is the theoretical size dependent splitting between the $\pm 1^L$ state and the ± 2 exciton ground state [see Fig. 2(d)].

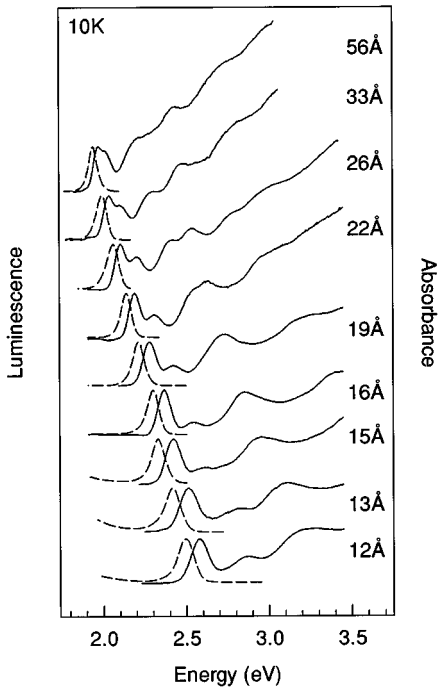

FIG. 8. Normalized absorption and full luminescence spectra for CdSe QD's between 12 and 56 Å in radius. A 300 W Xe arc lamp serves as the excitation source for both absorption and luminescence experiments. The excitation light is intentionally broad (50 nm FWHM) to prevent possible size selection of the dots. Detection of the transmission/luminescence signal is carried out with an OMA coupled to a 0.33 m spectrometer. The absorption spectra are indicated by solid lines; the corresponding luminescence spectra by dotted lines.

B. Stokes shift of the nonresonant photoluminescence

We have also studied the Stokes shift of the nonresonant photoluminescence. In this experiment we excite our samples above their band-edge absorption. The resulting ''full'' luminescence contains contributions from all crystallites in the sample residual size distribution and is inhomogeneously broadened. It shows no distinct phonon structure. This is unlike the FLN experiment where we suppress the inhomogeneous broadening of the luminescence by selectively exciting a narrow subset of crystallites. Figure 8 presents the full luminescence spectrum measured for nine sizes in the size series considered. As with the FLN data, the full luminescence shows a strong size dependence of the Stokes shift, ranging from ~ 100 meV for small sizes to ~ 25 meV for large sizes. Note that the full luminescence Stokes shift is taken to be the difference in energy between the lowest energy peak of the band-edge absorption and the peak of the full luminescence (the peak of the lowest energy absorption is determined by fitting the absorption spectra with a series of Gaussians). We denote the full luminescence Stokes shift as the ''nonresonant'' Stokes shift. The nonresonant Stokes shift requires too large a Huang-Rhys S parameter to be readily explained by exciton-phonon coupling.[43] There are, however, two other explanations which account for the large value of the nonresonant Stokes shift.

The first one is directly connected with the nanocrystal size distribution. In the strong confinement regime the total oscillator strength of transitions between the electron and hole quantum size levels does not depend on crystal size. However, the excitation probability is proportional to the number of participating states and, as a result, is proportional to the crystal volume and therefore to a^3, for excitations far from the band edge.[6] Thus while the first absorption peak generally follows the crystal size distribution, the position of the luminescence line for nonresonant excitation is determined by the largest crystals within this distibution. This causes a Stokes shift because the energy of the band-edge transitions in larger crystals is less than in smaller ones.

This, however, is not the main source of the nonresonant Stokes shift in our samples, which have a very narrow crystal size distribution ($<5\%$). The nonresonant Stokes shift here is connected with the band-edge exciton fine structure. In small nanocrystals the two upper states of the band-edge exciton fine structure possess nearly all the oscillator strength of the band-edge transition [see Fig. 4(d)], and the first absorption maximum is therefore determined by the positions of these two states. The nonresonant Stokes shift then is the difference in energy between these upper states and the ± 2 dark exciton ground state. This accounts for the sizable magnitude of the Stokes shift.

To describe the band-edge absorption we convolute the three optically active states with the intrinsic size distribution of the sample, weighted by their respective oscillator strengths. The peak of the band-edge absorption occurs at the weighted energetic mean of these states. We obtain the position of the full luminescence line by convoluting the position of the ± 2 dark exciton state with the size distribution weighted by the nanocrystal excitation probability ($\sim a^3$).

Figure 9 compares the shifts predicted by theory for a sample with a 5% size distribution to the experimental values of the nonresonant Stokes shift. The theory is shown as a

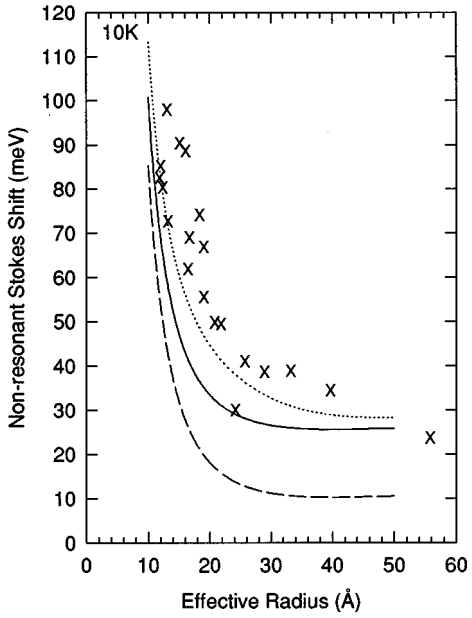

FIG. 9. The size dependence of the nonresonant Stokes shift. This Stokes shift is considered as the difference in energy between the peak of the band-edge absorption and the peak of the full luminescence. Experimental values are represented by $\times$. The dashed line is the theoretical Stokes shift calculated for a sample with a $\sigma=5\%$ size distribution. It is the difference between the mean energy of the three light exciton states and the mean position of the ± 2 exciton ground states of the participating crystals. The solid line includes the contribution of phonons to the theoretical splitting. The dotted line shows the theoretical results for a sample with a 10% size distribution

dashed line in the figure. We find a reasonable correlation between the two, but the theory underestimates the Stokes shift for the sizes considered. However, we have not taken into account phonons, whose role is seen experimentally in the LO phonon progressions observed in FLN and PLE spectra.[18,16,38,39] We include the contribution of phonons to the theoretical Stokes shift phenomenologically by including in the convolution with the size distribution the phonon dependent absorption and emission line shapes for single CdSe quantum dots. We assume the following forms for the absorption and emission line shapes:

$$A(\nu,\nu')=\sum_{l=1}^{3}\sum_{m=0}^{4}\frac{(S_a)^m}{\sqrt{2\pi}\gamma_{l,m}m!}\times\exp\left(\frac{-[\nu-(\nu'+\Delta_l+m\omega_{\mathrm{LO}})]^2}{2\gamma_{l,m}^2}\right), \quad (41)$$

$$E(\nu,\nu')=\sum_{n=0}^{4}\frac{(S_e)^n}{\sqrt{2\pi}\gamma_n n!}\exp\left(\frac{-[\nu-(\nu'-m\omega_{\mathrm{LO}})]^2}{2\gamma_n^2}\right). \quad (42)$$

We consider the first five LO phonon replicas associated with each of the three light exciton states (denoted by l) in absorption as well as the first five LO phonon replicas in emission. In Eqs. (42) and (43), ν' denotes the position of the zero phonon line, ω_{LO} is the LO phonon frequency separating the phonon replicas, Δ_l is the offset of the lth bright exciton from the $|F|=2$ dark exciton ground state, γ_n is the linewidth of the nth phonon replica in absorption and emission, and $\gamma_{l,m}$ is the width of the mth phonon replica for absorption into the lth light exciton state. The value $S_{a(e)}$ is the absorption (emission) exciton–LO-phonon coupling constant. It is equivalent to the Huang-Rhys S parameter assuming a displaced harmonic oscillator model.[40,41] The values we use for $S_{a(e)}$ are derived from experimental results.[41] Including the contribution of phonons moves the predicted band-edge absorption maximum to the blue and emission to the red, and results in the solid curve shown in Fig. 9. The modified curve still underestimates the nonresonant Stokes shift, but is in reasonable agreement with the experimental data.

We note that the nonresonant Stokes shift depends on the size distribution. This is illustrated in Fig. 9, where we show the increase of the calculated Stokes shift for a sample with a 10% size distribution. The good fit to the experimental data does not necessarily imply though that we have a 10% size distribution. Any other type of inhomogeneous broadening leads to an additional Stokes shift at the nonresonant excitation conditions. The nonresonant Stokes shift may contain contributions from shape distributions, structural inhomogeneities, and differences in chemical environment experienced by the dots dispersed in the glassy matrix.

C. Dark exciton lifetime in a magnetic field

Strong evidence for the dark exciton state is found in the study of the FLN spectra and luminescence decays in external magnetic fields. In Fig. 10(a) we show the magnetic field dependence of the FLN between 0 and 10 T for 12 Å radius dots. Each spectrum is normalized to the zero field one-phonon line for clarity. In isolation the ± 2 state would have an infinite lifetime within the electric dipole approximation, since the emitted photon cannot carry off an angular momentum of 2. However, the dark exciton can recombine via an LO phonon assisted momentum-conserving transition.[42] Spherical LO phonons with orbital angular momenta of 1 or 2 are expected to participate in these transitions; the selection rules are determined by the coupling mechanism.[8,43] Consequently, for zero field the LO phonon lines are strongly enhanced relative to the ZPL. With increasing magnetic field, however, the ± 2 level gains optically active ± 1 character [Eq. (30)], diminishing the need for LO phonon assisted recombination in dots whose hexagonal axis is not parallel to the magnetic field. This explains the dramatic rise of the ZPL intensity relative to the higher LO phonon replicas with increasing field.

The magnetic field induced admixture of the optically active ± 1 states shortens the exciton radiative lifetime. Luminescence decays for 12 Å radius crystallites between 0 and 10 T at 1.7 K are shown in Fig. 10(b). The sample was excited far to the blue of the first absorption maximum to avoid orientational selection in the excitation process since the transition dipole of the $|F|=1$ states is perpendicular to the c axis [see Eq. (27)]. Excitons rapidly thermalize to the ground state through acoustic and optical phonon emission. The long μs luminescence at zero field is consistent with LO phonon assisted recombination from this state. Although the light emission occurs primarily from the ± 2 state, its long radiative lifetime allows the thermally partially populated

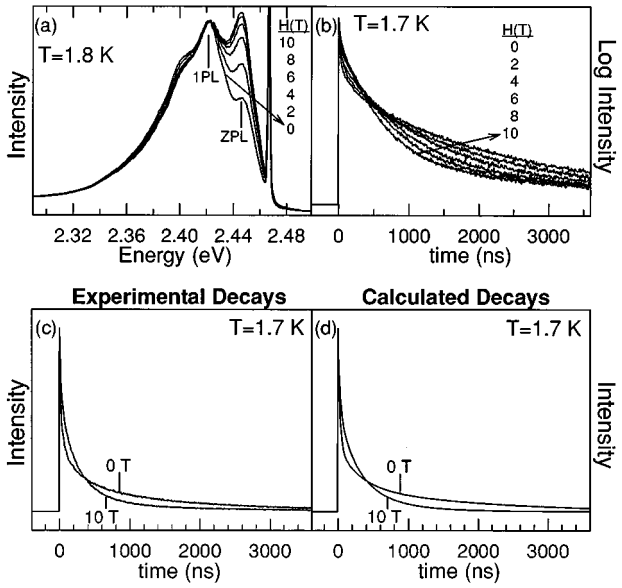

FIG. 10. (a) FLN spectra for 12 Å radius dots as a function of external magnetic field. The spectra are normalized to their one-phonon lines (1PL). A small fraction of the excitation laser, which is included for reference, appears as the sharp feature at 2.467 eV to the blue of the zero phonon line (ZPL). (b) Luminescence decays for 12 Å radius dots for magnetic fields between 0 and 10 T measured at the peak of the ''full'' luminescence (2.436 eV) and a pump energy of 2.736 eV. All experiments were done in the Faraday configuration ($\mathbf{H}\|\mathbf{k}$). (c) Observed luminescence decays for 12 Å radius dots at 0 and 10 T. (d) Calculated decays based on the three-level model described in the text. Three weighted three-level systems were used to simulate the decay at zero field with different values of γ_2 (0.033, 0.0033, and 0.000 56 ns^{-1}) and weighting factors (1, 3.8, and 15.3). γ_1 (0.1 ns^{-1}) and γ_{th} (0.026 ps^{-1}) were held fixed in all three systems.

$\pm 1^L$ state to also contribute to the luminescence. With increasing magnetic field the luminescence lifetime decreases; since the quantum yield remains essentially constant, we interpret this as an enhancement of the radiative rate.

The magnetic field dependence of the luminescence decays can be reproduced using three-level kinetics with $\pm 1^L$ and ± 2 emitting states.[16] The respective radiative rates from these states, $\Gamma_1(\theta,H)$ and $\Gamma_2(\theta,H)$, in a particular nanocrystal, depend on the angle θ between the magnetic field and the crystal hexagonal axis. The thermalization rate Γ_{th} of the $\pm 1^L$ state to the ± 2 level is determined independently from picosecond time resolved measurements. The population of the $\pm 1^L$ level is determined by microscopic reversibility. We assume that the magnetic field does not affect the zero magnetic field recombination but rather opens an additional channel for ground state recombination via admixture in the ± 2 state of the ± 1 states: $\Gamma_2(\theta,H)=\Gamma_2(0,0)+1/\tau_2(\theta,H)$. This also causes a slight decrease in the recombination rate of the $\pm 1^L$ state.

The decay at zero field is multiexponential, presumably due to sample inhomogeneities (e.g., in shape and symmetry breaking impurity contamimations). We describe the decay using three three-level systems, each having a different value of $\Gamma_2(0,0)$ and each representing a class of dots within the inhomogeneous distribution. These three-level systems are

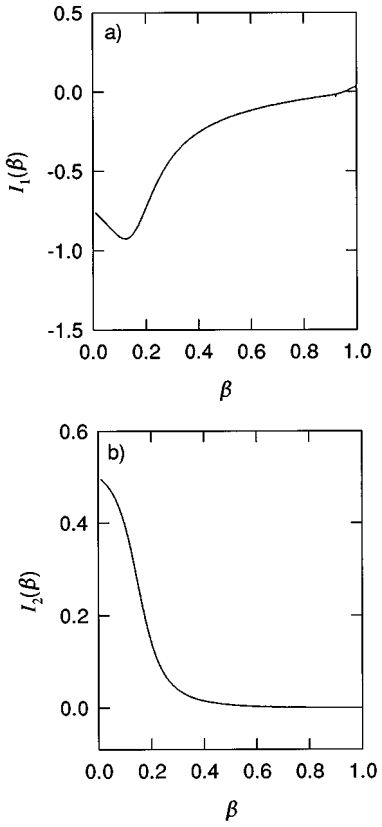

FIG. 11. Dependence of the hole radial function integrals I_1 and I_2, which enter in the expression for the hole g factor, on the hole effective mass ratio β.

then weighted to reproduce the zero field decay [Fig. 8(c)]. We obtain average values of $1/\Gamma_2(0,0)=1.42\ \mu\mathrm{s}$ and $1/\Gamma_1(0,0)=10.0$ ns, in good agreement with the theoretical value of the radiative lifetime for the $\pm 1^L$ state, $\tau_1^L=13.3$ ns, calculated for a 12 Å nanocrystal using Eq. (33).

In a magnetic field the angle dependent decay rates $[\Gamma_1(\theta,H),\Gamma_2(\theta,H)]$ are determined from Eq. (35). The field dependent decay is then calculated, averaging over all angles to account for the random orientation of the crystallite c axes. The simulated decay at 10 T [Fig. 8(c)], using the bulk value for $g_e=0.68$,[33] and the calculated values for Δ (19.4 meV) and η (10.3 meV) for 12 Å radius dots, is in excellent agreement with experiment. The hole g factor is treated as a fitting parameter since reliable values are not available. We used $g_h=-1.00$ consistent with theoretical estimates for this parameter, $g_h=-1.09$ (see the Appendix).

IV. DISCUSSION AND CONCLUSIONS

The size dependence of the Stokes shift we obtained for resonant excitation of the absorption band edge is in excellent agreement with the size dependence of the splitting between the lowest optically active bright exciton state and the optically passive dark exciton ground state. The discrepancy at the smallest sizes may be related to problems with the effective mass approximation at these sizes or to the increasing role played by phonons in the luminescence. The phonon interaction through the deformation potential was shown

both theoretically[44] and experimentally[45] to increase with decreasing size. This can lead to the formation of an exciton-polaron and be a source of an additional Stokes shift of the luminescence.[36]

The large difference between the resonant excitation Stokes shift and the Stokes shift of the nonresonant photoluminescence is related to the difference in the oscillator strengths of the upper and lower optically active bright exciton states. In the smallest crystals, the upper bright excitons gain the oscillator strength of the lower bright excitons and give the main contribution to the absorption. The nonresonant Stokes shift in this case is the energy difference between the upper bright excitons and the optically passive dark exciton ground state. The experimental size dependence of the nonresonant Stokes shift is in reasonable agreement with the theory. What discrepancy there is may be attributed to phonon participation in the luminescence, which is not well understood theoretically for CdSe nanocrystals.[46]

While the surface effects previously invoked to explain the photophysical behavior of CdSe quantum dots may still play a role, especially via nonradiative processes, the energetics and dynamics of the band-edge emission can be quantitatively understood in terms of the intrinsic band-edge exciton structure. Exciton thermalization to a dipole forbidden ± 2 dark exciton state resolves the issue of the long lifetimes of the band-edge luminescence. An external magnetic field mixes the dark exciton with the optically active bright exciton states and allows its recombination. The magnetic field dependence of the emission decays and the observed LO phonon structure confirm the presence of this ''dark'' excitonic state.

In zero external magnetic field, recombination of the ± 2 dark exciton can take place via a LO phonon assisted transition. Phonons can take up part of the total angular momentum projection, ± 2, which cannot be taken up by a photon alone. However, even in the absence of an external magnetic field the zero LO phonon line is weakly allowed, suggesting an alternate recombination pathway, for example, through coupling to acoustic phonons. Interaction with paramagnetic defects in the lattice can also provide an important additional mechanism for recombination. The spins of these defects potentially generate strong effective internal magnetic fields, which, depending on the strength of the spin-spin exchange interaction with the carriers and on the crystal radius, can reach several tens of teslas, and induce spin-flip assisted transitions of the ± 2 state, enabling zero phonon recombination to occur. Preliminary electron paramagnetic resonance (EPR) spectra do in fact indicate a small concentration of paramagnetic centers in our samples, and efforts under way to introduce an electrically neutral magnetic impurity such as Mn^{2+} into the lattice may confirm this mechanism.

In spite of the obvious success of our model in describing the electronic structure of the band-edge excitation in CdSe nanocrystals, several questions remain unanswered. These include the increase with decreasing size of the homogeneous exciton absorption line width[47] and the underestimation of the Stokes shift at small sizes. Both issues may be connected to our lack of knowledge about the main mechanism of exciton interaction with polar optical phonons.[46]

In conclusion, we have described the band-edge exciton fine structure, and have explained in a self-consistent way most of the complex and controversial experimental data in nanosize CdSe quantum dots, e.g., the small Stokes shift of the resonant photoluminescence, the large Stokes shift of the nonresonant PL relative to the band-edge absorption maxima, the long radiative lifetime, its decrease in magnetic fields, and the fine structure of the photoluminescence line narrowing and photoluminescence excitation spectra.[18]

ACKNOWLEDGMENTS

M.N. and D.J.N. benefited from AT&T and NSF financial support, respectively. M.G.B. thanks the Lucille and David Packard Foundation and the Alfred P. Sloan Foundation for financial support. This work was funded in part by the MIT Center for Materials Science and Engineering (NSF Grant No. DMR-90-22933) and by NSF (DMR-91-57491). We also thank the MIT Harrison Spectroscopy Laboratory (NSF Grant No. CHE-93-04251) for the use of their facilities.

APPENDIX: CALCULATION OF THE HOLE *g* FACTOR

The expression for the g factor of a hole localized in a spherically symmetric potential was obtained by Gel'mont and D'yakonov:[34]

$$g_h=\frac{4}{5}\gamma_1 I_2+\frac{8}{5}\gamma(I_1-I_2)+2\kappa\left(1-\frac{4}{5}I_2\right), \qquad \text{(A1)}$$

where γ_1, γ, and κ are the Luttinger parameters[48] and $I_{1,2}$ are integrals of the hole radial wave functions [see Eq. (6)]:

$$I_1=\int_0^a drr^3R_2\frac{dR_0}{dr}, \quad I_2=\int_0^a drr^2R_2^2. \qquad \text{(A2)}$$

These integrals depend only on the parameter β, and their variation with β is shown in Fig. 11. Using $\gamma_1=2.04$ and $\gamma=0.58$,[5] and the relationship $\kappa=-2/3+5\gamma/3-\gamma_1/3$,[49] one calculates that $g_h=-1.09$.

[1] C. R. Pidgeon and R. N. Brown, Phys. Rev. **146**, 575 (1966).

[2] R. L. Aggarwal, in *Modulation Techniques*, edited by by R. K. Willardson and A. C. Beer, Semiconductors and Semimetals Vol. 9 (Academic Press, New York, 1974), p. 151.

[3] A. I. Ekimov, F. Hache, M. C. Schanne-Klein, D. Ricard, C. Flytzanis, I. A. Kudryavtsev, T. V. Yazeva, A. V. Rodina, and Al. L. Efros, J. Opt. Soc. Am. B **10**, 100 (1993).

[4] D. J. Norris, A. Sacra, C.B. Murray, and M. G. Bawendi, Phys. Rev. Lett. **72**, 2612 (1994).

[5] D. J. Norris and M. G. Bawendi, Phys. Rev. B **53**, 16 338 (1996).

[6] Al. L. Efros and A. L. Efros, Fiz. Tekh. Poluprovodn. **16**, 1209 (1982) [Sov. Phys. Semicond. **16**, 772 (1982)].

[7] L. E. Brus, J. Chem. Phys. **80**, 4403 (1984).
[8] Al. L. Efros, Phys. Rev. B 46, 7448 (1992).
[9] G. B. Grigoryan, E. M. Kazaryan, Al. L. Efros, and T. V. Yazeva, Fiz. Tverd. Tela **32**, 1772 (1990) [Sov. Phys. Solid State **32**, 1031 (1990)].
[10] A. I. Ekimov, Phys. Scr. **39**, 217 (1991).
[11] P. A. M. Rodrigues, G. Tamulaitis, P. Y. Yu, and S. H. Risbud, Solid State Commun. **94**, 583 (1995).
[12] M. G. Bawendi, W. L. Wilson, L. Rothberg, P. J. Carroll, T. M. Jedju, M. L. Stegerwald, and L. E. Brus, Phys. Rev. Lett. **65**, 1623 (1990).
[13] M. O'Neil, J. Marohn, and G. McLendon, J. Phys. Chem. **94**, 4356 (1990); A. Hasselbarth, A. Eychmuller, and H. Weller, Chem. Phys. Lett. **203**, 271 (1993).
[14] P. D. J. Calcott, K. L. Nash, L. T. Canham, M. J. Kane, and D. Brumhead, J. Lumin. **57**, 257 (1993).
[15] M. Chamarro, C. Gourdon, P. Lavallard, and A. I. Ekimov, Jpn. J. Appl. Phys. **34**, Suppl. 34-1, 12 (1995).
[16] M. Nirmal, D. J. Norris, M. Kuno, M. G. Bawendi, Al. L. Efros, and M. Rosen, Phys. Rev. Lett. **75**, 3728 (1995).
[17] M. Chamarro, C. Gourdon, P. Lavallard, O. Lublinskaya, and A. I. Ekimov, Phys. Rev. B **53**, 1 (1996).
[18] D. J. Norris, Al. L. Efros, M. Rosen, and M. G. Bawendi, Phys. Rev. B **53**, 16 347 (1996).
[19] J. M. Luttinger and W. Kohn, Phys. Rev. **97**, 869 (1955).
[20] Such optically passive exciton states were first observed in magnetic fields by J. B. Stark, W. H. Knox, and D. S. Chemla, Phys. Rev. B **46**, 7919 (1992).
[21] A. I. Ekimov, A. A. Onushchenko, A. G. Plukhin, and Al. L. Efros, Zh. Éksp. Teor. Fiz. **88**, 1490 (1985) [Sov. Phys. JETP **61**, 891 (1985)].
[22] J. B. Xia, Phys. Rev. B **40**, 8500 (1989).
[23] K. J. Vahala and P. C. Sercel, Phys. Rev. Lett. **65**, 239 (1990); P. C. Sercel and K. J. Vahala, Phys. Rev. B **42**, 3690 (1990).
[24] Al. L. Efros and A. V. Rodina, Solid State Commun. **72**, 645 (1989).
[25] G. L. Bir and G. E. Pikus, *Symmetry and Strain-Induced Effects in Semiconductors* (Wiley, New York, 1975).
[26] Al. L. Efros and A. V. Rodina, Phys. Rev. B **47**, 10 005 (1993)
[27] L. E. Brus (unpublished).
[28] E. I. Rashba, Zh. Éksp. Teor. Fiz. **36**, 1703 (1959) [Sov. Phys. JETP **9**, 1213 (1959)].
[29] V. P. Kochereshko, G. V. Mikhailov, and I. N. Ural'tsev, Fiz. Tverd. Tela **25**, 759 (1983) [Sov. Phys. Solid State **25**, 439 (1983)].
[30] In accordance with SAXS and TEM measurements the ellipticity was approximated by the polynomial $\mu(a)=0.101-0.034a+3.507\times10^{-3}a^2-1.177\times10^{-4}a^3+1.863\times10^{-6}a^4-1.418\times10^{-8}a^5+4.196\times10^{-11}a^6$.
[31] C. B. Murray, D. J. Norris, and M. G. Bawendi, J. Am. Chem. Soc. **115**, 8706 (1993).
[32] M. G. Bawendi, P. J. Carroll, W. L. Wilson, and L. E. Brus, J. Chem. Phys. **96**, 946 (1992).
[33] W. W. Piper, in *Proceedings of the 7th International Conference on II-VI Semiconductor Compounds, Providence, RI*, edited by D. G. Thomas (Benjamin, New York, 1967), p. 839.
[34] B. L. Gel'mont and M. I. D'yakonov, Fiz. Tekh. Poluprovodn. **7**, 2013 (1973) [Sov. Phys. Semicond. **7**, 1345 (1973)].
[35] L. D. Landau and E. M. Lifshitz, *Relativistic Quantum Theory*, 2nd ed. (Pergamon Press, Oxford, 1965).
[36] T. Itoh, M. Nishijima, A. I. Ekimov, C. Gourdon, Al. L. Efros, and M. Rosen, Phys. Rev. Lett. **74**, 1645 (1995).
[37] S. Nomura and T. Kobayashi, Solid State Commun. **82**, 335 (1992).
[38] M. Nirmal, C. B. Murray, D. J. Norris, and M. G. Bawendi, Z. Phys. D **26**, 361 (1993).
[39] M. Nirmal, C. B. Murray, and M. G. Bawendi, Phys. Rev. B **50**, 2293 (1994).
[40] S. Schmitt-Rink, D. A. B. Miller, and D. S. Chemla, Phys. Rev. B **35**, 8113 (1987).
[41] The values of $S_e=0.45$ and $S_a=0.14$ are consistent with experimental measurements (Ref. 18).
[42] P. D. J. Calcott, K. J. Nash, L. T. Canham, M. J. Kane, and D. Brumhead, J. Phys. Condens. Matter **5**, L91 (1993).
[43] M. C. Klein, F. Hache, D. Ricard, and C. Flytzanis, Phys. Rev. B **42**, 11 123 (1990).
[44] T. Takagahara, Phys. Rev. B **47**, 4569 (1993).
[45] J. J. Shiang, S. H. Risbud, and A. P. Alivisatos, J. Chem. Phys. **98**, 8432 (1993); J. J. Shiang, R. K. Grubbs, and A. P. Alivisatos (unpublished); J. J. Shiang, A. P. Alivisatos, and K. B. Whaley (unpublished).
[46] Al. L. Efros, in *Phonons in Semiconductor Nanostructures*, edited by J.-P. Leburton, J. Pascual, and C. Sotomayor-Torres (Kluwer Academic Publishers, Boston, 1993), p. 299.
[47] D. J. Norris, M. Nirmal, A. Sacra, C.B. Murray, and M. G. Bawendi, Z. Phys. D **26**, 355 (1993).
[48] J. M. Luttinger, Phys. Rev. **102**, 1030 (1956).
[49] G. Dresselhaus, A. F. Kip, and C. Kittel, Phys. Rev. **98**, 368 (1955).